Journal of Molecular Structure 1252 (2022) 132090

Contents lists available at ScienceDirect

Journal of Molecular Structure

journal homepage: www.elsevier.com/locate/molstr

A new 3-substituted BODIPY dye: Synthesis, crystal structure, photophysical, non-linear optic and OLED properties

Hilal Kırpık[a,*], Sultan Erkan[b], Muhammet Kose[a,*]

[a] Chemistry Department, Kahramanmaras Sutcu Imam University, Kahramanmaras 46100, Turkey
[b] Department of Chemistry, Faculty of Science, Cumhuriyet University, Sivas 58140, Turkey

ARTICLE INFO

Article history:
Received 4 October 2021
Revised 22 November 2021
Accepted 3 December 2021
Available online 6 December 2021

Keywords:
BODIPY
Structural characterization
Photophysical property
Absorption
Emission

ABSTRACT

A BODIPY derivative (compound **2**), substituted with 4-nitrophenyl at the *meso* position and its 3-pyrrole substituted derivative (compound **3**) were synthesized and characterized. The structure of compound **3** was elucidated by single crystal X-ray diffraction study. The Photophysical properties of compounds **2** and **3** were studied in various solvents with different polarities. The expansion of the π-conjugation by introduction of the pyrrole ring to 3-position of the BODIPY core results in a considerable red shift in the absorption and emission bands. Also, photophysical properties of compounds **2** and **3** was affected by the solvent polarity. Compound **3** showed stronger fluorescence in non-polar solvents (Φ_F = 0.049 in Hexane). In order to establish the effect of the pyrrole attachment, the synthesized compounds **2** and **3** were optimized at the level of computational chemistry, DFT/B3LYP/6–31+*G*(d,p). The highest occupied molecular orbital energy (EHOMO), the lowest unoccupied molecular orbital (ELUMO), the energy gap (ΔE) parameters and contour diagrams obtained from the optimized structures were investigated. The nonlinear optical (NLO) and light emission (OLED) properties of the compounds were investigated computationally on the basis of polarizability parameters and Marcus theory, respectively.

1. Introduction

4,4-Difluoro-4-bora-3a,4a-diaza-s-indacene (BODIPY) derivatives are an important class of fluorophores due to their many excellent properties including high thermal and photochemical stabilities, good solubility, sharp absorption and emission bands in the visible region, high fluorescence quantum yields and molar absorption coefficients and negligible triplet-state formation [1–4]. Another attractive feature of BODIPY derivatives is their tunable spectroscopic and photophysical properties [5–7]. Thanks to all outstanding properties of BODIPY derivatives, they have found applications in a wide variety of research fields such as fluorescent sensors [2,3,8–14], biological labels [15,16] and probs [17–20], tunable laser dyes [21–23], sensitizers for solar cells [24,25]. Recently, BODIPY derivatives have also been investigated as an acceptor unit for organic OLED applications [26–28]. For various applications of BODIPY derivatives, their spectroscopic and photophysical properties can be tuned by changing the substituents of different electron densities or by adjusting conjugation length, or via chemical modification at suitable positions of the BODIPY core [29–34]. The incorporation of new substituents at the 3- and 5-positions of BODIPY core has a large impact on the spectroscopic and photophysical properties [1,2]. This approach has attracted great interest especially in the design of new BODIPY-based fluorescent labels and sensors for biological applications [2,35–37]. BODIPY derivatives can also serve as NLO materials by extending π- conjugation and introducing appropriate electron donor or acceptor groups for forming Intramolecular Charge Transfer [38–40]. The direct attachment of pyrrole at 3-position of the BODIPY core has been proven cause to red shift in the absorption and emission maxima. 3-pyrrolyl BODIPY derivatives including various substituent except -NO_2 at the *meso*–aryl group were synthesized and their spectroscopic properties were investigated [41–43]. Kaur et al. also showed that 3-pyrrolyl BODIPY derivatives can be functionalized with various functional groups from the α-position of the added pyrrole ring and they can be used in the synthesis of new BODIPY derivatives [34]. Furthermore, pyrrole-containing BODIPY derivatives such as BODIPY 576/589 and BODIPY 650/665 are commercially available as biological labels [44]. Consequently, pyrrole-containing BODIPY derivatives can be suitable candidates for detection of biological species. In this context investigation of their structures and photophysical properties will be helpful in design of new BODIPY-based fluorescent labels and sensors for biological applications.

* Corresponding authors.
E-mail addresses: hilalkirpik@gmail.com (H. Kırpık), muhammetkose@ksu.edu.tr (M. Kose).

https://doi.org/10.1016/j.molstruc.2021.132090
0022-2860/

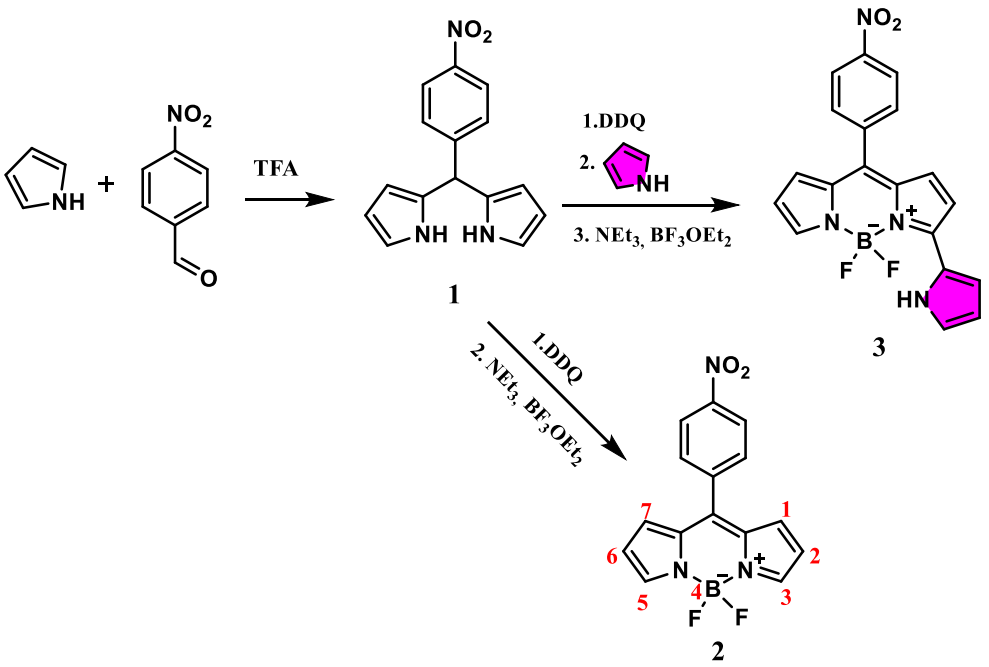

Fig. 1. Synthesis scheme of compounds **2** and **3**.

In the current work, we synthesized a new pyrrole substituted BODIPY derivative (compound **3**) (Fig. 1) and its molecular structure was characterized X-ray diffraction studies. Moreover, the absorption and emission properties were investigated in different solvents. The effect of the pyrrole attachment to 3-position of one of the BODIPY core on the photophysical properties were examined. In order to establish the effect of the pyrrole attachment, HOMO-LUMO calculations were performed. Finally, non-linear optic and OLED properties of BODIPY derivatives compounds **2** and **3** were investigated.

2. Experimental

2.1. General

Starting materials (triethylamine, 4-nitrobenzaldehyde, 2,3-dichloro-5,6-dicyano-1,4-benzoquinone, NaOH, Na_2SO_4) were purchased from commercial sources and used as received. Dichloromethane was distilled over CaH_2. Freshly distilled pyrrole was used in the synthesis. FT-IR spectra were measured on a Perkin Elmer Spectrum 100 FT-IR. The UV–Vis. absorption spectra were taken on a Perkin Elmer Lambda 45 spectrophotometer. The photoluminescence spectra of compounds were obtained on a Perkin Elmer LS55 luminescence spectrometer.

2.2. Determination of the fluorescence quantum yield

Fluorescence quantum yield (Φ_F) of compound **3** were determined employing the comparative method according to followed Equation where r and s refer to reference and sample, respectively [45]. *m* is gradient of the plots of integrated fluorescence intensities against absorbances and n is the refractive index of solvent.

$$\Phi_s = \Phi_r(m_s/m_r)(n_s/n_r)^2$$

Rhodamine B was used as a reference (Φ_F = 0.68 in EtOH) [46]. Absorption and emission spectra of reference and sample were measured three different concentrations with absorbance values < 0.1 under identical conditions. The reference and the sample were excited at the same wavelength.

2.3. Synthesis of the meso–(4-nitrophenyl)dipyrromethane (*1*)

The *meso*–(4-Nitrophenyl) dipyrromethane (compound **1**) was synthesized according to the reported method [47]. Pyrrole (25 mL, 25 eqv.) and 4-nitrobenzaldehyde (2.18 g, 1 eqv.) were stirred under N_2 atmosphere at room temperature for 5 min. To the reaction mixture, one drop trifluoroacetic acid was added and then the reaction mixture was stirred further 5 min under the same conditions. The reaction mixture was treated with 0.1 M NaOH and then extracted by ethyl acetate. The combined organic layer was washed with water and dried over Na_2SO_4. The solvent was removed on a rotary evaporator to give an orange coloured oil. The crude product was crystallised in ethyl acetate-hexanes and then re-crystallised from EtOH to give target compound **1** as yellow-green crystals.

1: $C_{15}H_{13}N_3O_2$ MW: 267.29 g/mol, Yield: 40% (1.540 g), Mp: 154–158 °C FT-IR (ATR, cm^{-1}): 3393, 3357, 1590, 1510, 1344, 1250, 1113, 1092, 1028, 803, 777, 740, 725 cm^{-1}. ^1H NMR (400 MHz, $CDCl_3$) δ = 8.18 (d, 2H, CH_{phenyl}), 8.00 (bs, 2H, -NH), 7.39 (d, 2H, CH_{phenyl}), 6.77 (s, 2H, -$CH_{pyrrole}$), 6.21 (s, 2H, -$CH_{pyrrole}$), 5.90 (s, 2H, -$CH_{pyrrole}$), 5.60 (s, 1H, -CH_{meso}). ^{13}C NMR (100 MHz, $CDCl_3$): δ = 149.68, 146.93, 130.82, 129.25, 123.81, 117.98, 108.82, 107.84, 43.82 ppm.

2.4. Synthesis of the 4,4-difluoro-8-(4-nitrophenyl)–4-bora-3a,4a-diaza-s-indacene (*2*)

Compound **2** was synthesized using adapted literature methods [48,49]. Compound **1** (0.50 mmol, 0.134 g) was dissolved in dry CH_2Cl_2 (50 mL) and then 2,3-dichloro-5,6-dicyano-1,4-benzoquinone (0.75 mmol, 0.170 g, 10 mL dry CH_2Cl_2) was added dropwise. The reaction mixture was stirred under N_2 atmosphere for 30 min at room temperature. To the reaction mixture, triethylamine (2.8 mL) and $BF_3{\cdot}OEt_2$ (3.1 mL) were added and then the reaction mixture was further stirred for 2 h under N_2 atmosphere at room temperature. Then the reaction mixture was washed with water and brine. The combined organic layer dried over Na_2SO_4 and concentrated under reduced pressure. The crude product was purified by silica-gel column chromatography using DCM/petrol (2:1) as eluent to obtain compound **2** as a red solid.

2: $C_{15}H_{10}BF_2N_3O_2$ MW: 313.07 g/mol, Yield: 50% (0.078 g), Mp: 264–270 °C FT-IR (ATR, cm^{-1}): 3106, 1603, 1524, 1480, 1412, 1404, 1377, 1348, 1288, 1255, 1226, 1170, 1155, 1099, 1076, 1048, 1011, 978, 910, 866, 850, 775, 746, 723 cm^{-1}. ^1H NMR (400 MHz, $CDCl_3$) δ = 8.42 (d, 2H), 8.01 (s, 2H), 7.77 (d, 2H), 6.87 (s, 2H), 6.61 (s, 2H). ^{13}C NMR (101 MHz, $CDCl_3$): δ = 149.13, 145.56, 143.78, 139.79, 134.53, 131.25, 123.69, 119.32 ppm.

2.5. Synthesis of the 3-pyrrolyl-4,4-difluoro-8-(4-nitrophenyl)−4-bora-3a,4a-diaza-s-indacene (**3**)

Compound **3** was synthesized according to the reported method [41]. Compound *1* (1.35 mmol, 0.361 g) was dissolved in $CHCl_3$ (30 mL) and then 2,3-dichloro-5,6-dicyano-1,4-benzoquinone (3.37 mmol, 0.765 g) was added and the reaction mixture was stirred for 30 min at room temperature. To the reaction mixture, pyrrole (4.0 mmol) was added and the reaction mixture stirred for 15 min. Then triethylamine (54 mmol) and $BF_3{\cdot}OEt_2$ (67.5 mmol) were added and the reaction mixture stirred for 30 min at 50 °C. The reaction mixture was poured into CH_2Cl_2 and then washed with 0.1 M NaOH solution and water. The combined organic layer dried over Na_2SO_4 and concentrated under reduced pressure. The crude product was purified by silica-gel column chromatography using DCM/hexane (2: 1) as eluent to obtain compound **3** as a purple solid. This compound was crystallised in DCM-hexane to give as purple crystals.

3: $C_{15}H_{10}BF_2N_3O_2$ MW: 378.15 g/mol, Yield: 10% (0.051 g), FT-IR (ATR, cm^{-1}): 3395, 2953, 2919, 2850, 1728, 1574, 1558, 1501, 1461, 1410, 1377, 1345, 1286, 1267, 1226, 1171, 1136, 1106, 1070, 1031, 987, 823, 787, 743, 720 cm^{-1}. ^1H NMR (400 MHz, $CDCl_3$) δ 10.62 (bs, 1H, -NH), 8.41(d, 2H), 7.74 (m, 2H), 7.56(m, 2H), 7.12(s, 1H), 7.00 (d, 1H), 6.88 (d, 1H), 6.57 (m, 1H), 6.51(m, 1H), 6.47 (m, 1H). ^{13}C NMR (101 MHz, $CDCl_3$) δ 167.79, 152.67, 148.41, 142.70, 140.95, 139.36, 137.04, 135.49, 132.45, 132.37, 131.31, 130.77, 128.95, 127.58, 123.57, 122.31, 119.84, 116.46, 113.92, 112.16. ESI-Q-$TOF_{(m/z)}$: 391.2900 $[M+H]^+$, 391.29 $[M\text{-}F+CH_3OH]^+$, 413.2728 $[M+CH_3OH+H]^+$.

2.6. X-ray crystallography

A suitable crystal of compound **3** was selected and X-ray diffraction data were collected on a Bruker APEX 2 CCD diffractometer. The crystal was kept at 293(2) K during data collection. Using Olex2 [50], the structure was solved with the SHELXT [51] structure solution program using Intrinsic Phasing and refined with the SHELXL [52] refinement package using Least Squares minimisation. Hydrogen atoms bonded to carbon and nitrogen atoms are located at the appropriate positions using a riding model. X-ray crystallographic data and refinement details are given in Table 1. Bond lengths/angles (Tables S1 and S2) and hydrogen bond parameters (Table S3) are provided in the supplementary documents.

2.7. Computational method

The three-dimensional structures of the molecules were created with the program Gauss-View 6.0.0 [53]. Gaussian 09 AML64L-Revision C.01 [54] was used in the calculations. All calculations were performed at 6–31+*G*(d,p). The highest occupied molecular orbital energy (EHOMO), lowest unoccupied molecular orbital energy (ELUMO) and energy gap (ΔE) were found by using Eqs. (1)–(3) [55].

$$I = -E_{HOMO} \tag{1}$$

$$A = -E_{LUMO} \tag{2}$$

Table 1
X-ray crystallographic data and refinement details for 3.

Identification code	3
Empirical formula	$C_{19}H_{13}N_4O_2BF_2$
Formula weight	378.14
Temperature/K	293(2)
Crystal system	Triclinic
Space group	P-1
a/Å	7.7490(7)
b/Å	9.5207(7)
c/Å	12.9045(10)
α/°	75.236(7)
β/°	83.162(7)
γ/°	70.346(7)
Volume/Å^3	866.39(13)
Z	2
Crystal size/mm^3	0.15 × 0.1 × 0.08
Radiation	MoKα (λ = 0.71073)
2Θ range for data collection/°	7.106 to 57.764
Index ranges	$-10 \le h \le 9$, $-12 \le k \le 12$, $-15 \le l \le 17$
Reflections collected	6621
Independent reflections	3901 [R_{int} = 0.0239, R_{sigma} = 0.0534]
Data/restraints/parameters	3901/0/253
Goodness-of-fit on F^2	1.018
Final R indexes [$I>=2\sigma$ (I)]	R_1 = 0.0518, wR_2 = 0.1163
Final R indexes [all data]	R_1 = 0.0918, wR_2 = 0.1396
Largest diff. peak/hole / e Å^{-3}	0.20/−0.27
CCDC	2,110,205

$$\Delta E = E_{LUMO} - E_{HOMO} \tag{3}$$

For NLO properties, total static dipole moment (μ), average polarizability (α), anisotropy of polarizability ($\Delta\alpha$) and total static first hyperpolarizability (β) are calculated from Eqs. (4)–(7) [56].

$$\mu = \left(\mu_x{}^2 + \mu_y{}^2 + \mu_z{}^2\right)^{1/2} \tag{4}$$

$$a = \frac{1}{3}(a_{xx} + a_{yy} + a_{zz}) \tag{5}$$

$$\Delta a = \frac{1}{\sqrt{2}}\left[(a_{xx} - a_{yy})^2 + (a_{yy} - a_{zz})^2 + (a_{zz} - a_{xx})^2 + 6a_{xz}{}^2 + 6a_{xy}{}^2 + 6a_{yz}{}^2\right]^{1/2} \tag{6}$$

$$\beta = \left[(\beta_{xxx} + \beta_{xyy} + \beta_{xzz})^2 + (\beta_{yyy} + \beta_{yzz} + \beta_{yxx})^2 + (\beta_{zzz} + \beta_{zxx} + \beta_{zyy})^2\right]^{1/2} \tag{7}$$

OLED properties were investigated under the Marcus theory. The Marcus equation is shown in Eq. (8). Thanks to this equation, rate constants for electron or hole transfer of molecules can be calculated [57].

$$k_{C\tau} = \frac{2\pi}{h} t^2 \sqrt{\frac{1}{4\pi\lambda k_B T}} \exp\left[-\frac{\lambda + \Delta G^0}{4\lambda k_B T}\right] \tag{8}$$

Where k_{CT} is the charge transfer rate constant, t is the charge transfer integral for electron or hole, $\hbar$ is the induced Planck constant, λ is the reorganization energy for electron or hole, k_B is the Boltzmann constant, T is the temperature, $\Delta G°$ is the free energy of the transfer reaction.

The reorganization energies (λ) are considered as two different parameters, the external reorganization energy (λ_{ext}) and the internal reorganization energy (λ_{int}). λ_{ext} indicates the effect of polarized medium on charge transfer, and λ_{int} is a measure of the

structural change between ionic and neutral states. In computational chemistry studies, the λ_{int} argument is taken into account. The reorganization energies, electron (λ_e) and hole (λ_h) reorganization energy, are found from the single point energy of the compounds. Cationic and anionic species are produced from the optimized structure of the compounds studied to calculate their rearrangement energies. For these species, single point energy calculations are made at the B3LYP/6–31+*G*(d,p) level. Using the calculated single point energies of neutral, cationic and anionic species, the reorganization energies for electron and hole are calculated from Eqs. (9), (10) [58–60].

$$\lambda e = \left(E_0^- - E_-^-\right) + \left(E_-^0 - E_0^0\right) \quad (9)$$

$$\lambda_h = \left(E_0^+ - E_+^+\right) + \left(E_+^0 - E_0^0\right) \quad (10)$$

where E_0^+ and E_0^- are the energies of the cation and anion composed of neutral molecule. E_+^+ and E_-^- are the energies of the cation and anion obtained from cation and anion. E_+^0 and E_-^0 are the energy of the neutral molecule calculated at the cationic and anionic state. E_0^0 is the energy of the neutral molecule at the ground state.

Another parameter that provides the theoretical prediction of OLED properties are adiabatic/vertical ionization potentials (IPa/IPv) and adiabatic/vertical electron affinities (EAa/EAv) [61]. These mentioned parameters can be calculated from Eqs. (11) to (14).

$$IPa = E_+^+ - E_0^0 \quad (11)$$

$$IPv = E_0^+ - E_0^0 \quad (12)$$

$$EAa = E_0^0 - E_-^- \quad (13)$$

$$EAv = E_0^0 - E_0^- \quad (14)$$

Here E_0^- and E_0^+ are the energy of the re-optimized anion (cation) derived from the optimized structure of the neutral molecule. E_-^- (E_+^+) is the energy of the anion (cation) calculated with the optimized anion (cation) structure, E_-^0 (E_+^0) is the energy of the neutral molecule calculated at the anionic (cationic) state. In addition, $E_0^0$is defined as the energy of the neutral molecule at the ground state [62].

3. Results and discussion

In this study, BODIPY derivatives (compounds **2** and **3**) were synthesized as shown in Fig. 1. Dipyrromethane compound **1** was obtained from the acid-catalyzed reaction of 4-nitro benzaldehyde with pyrrole. To obtain compound **2**, compound **1** was first oxidized by DDQ and then reacted with $BF_3{\cdot}OEt_2$ at room temperature. After compound **1** was oxidized by DDQ, pyrrole was added to the reaction mixture and then complexation with $BF_3.OEt_2$ to get desired compound **3**. Synthesized compounds **1**–**3** are soluble in common organic solvent such as hexane, dichloromethane chloroform, ethanol, acetonitrile and dimethyl sulfoxide.

Compounds **1** and **2** were already synthesized in the literature [47–49]. We characterized these compounds by spectroscopic techniques such as FT-IR and NMR (^{1}H and ^{13}C NMR) spectroscopies. Synthesized compound **3** was characterized by spectroscopic techniques such as FT-IR, NMR (^{1}H and ^{13}C NMR) and mass spectroscopies. FT-IR spectra of compounds **1**–**3** between 4000 and 400 cm^{-1} are given Fig. S1. The FT-IR spectrum of compound **1** shows stretching peaks around at 3357 cm^{-1} assigned to the N-H stretching's. In the spectrum of compound **2**, the N-H stretching peak disappeared and B-F vibrations were observed in the range of 978–1099 cm^{-1} [63]. A new peak was observed at 3395 cm^{-1} in the FT-IR spectrum of compound **3** and it was assigned to the N-H stretching resulting from the pyrrole attachment at 3-position of BODIPY core. The ^{1}H NMR spectra of compound **1**–3 were measured in $CDCl_3$. The spectral data are presented in the experimental section and spectra are given Fig. S2-S4. In the spectrum of compound **1**, -NH protons were observed as a broad singlet signal at 8.00 ppm; the meso–aryl protons appeared as doublet signals at 8.18 and 7.39 ppm. The pyrrolic protons of compound **2** were observed as singlet signals between 5.90–6.77 ppm and -CH_{meso} proton signal appeared as a singlet signal at 5.60 ppm. Upon the complexation of compound **1** with BF_2, -NH and -CH_{meso} protons of compound **1** disappeared in the spectrum of compound **2**. In the spectrum of compound **3**, -NH proton of pyrrole ring was observed at 10.62 ppm. Furthermore, ESI-Q-TOF mass spectrum of compound **3** was measured in methanol. The peaks at m/z 391.2900 and 413.2728 were assigned to the molecular ions $[M+H]^+$ and $[M+CH_3OH+H]^+$, respectively (Fig. S5).

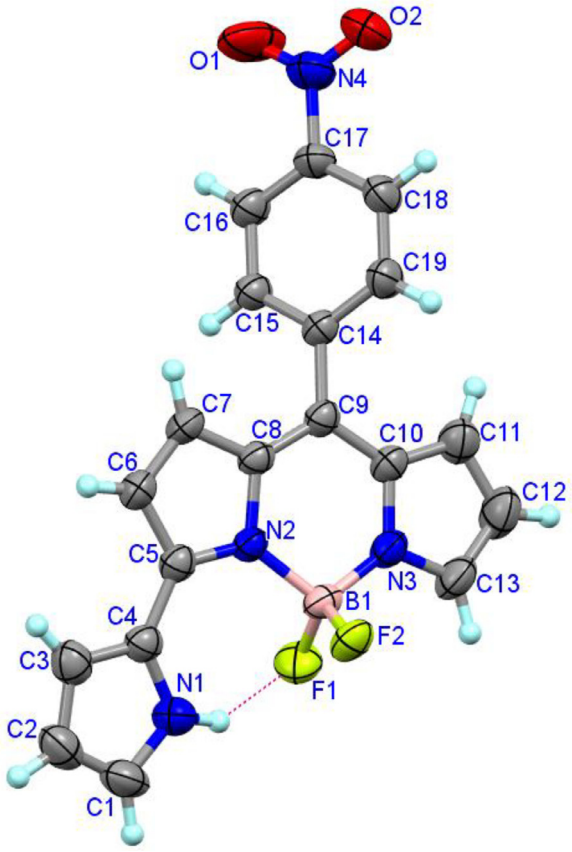

Fig. 2. Molecular structure of compound **3** with atom numbering (thermal ellipsoid with 50% probability).

3.1. Molecular structure 3

Single crystals of compound **3** were obtained from slow evaporation of the compound in DCM and crystal structure of the compound was investigated by X-ray diffraction study. The structure of the compound was solved in *triclinic* unit cell P-1 space group. Molecular structure of the compound with atom numbering is shown in Fig. 2. In the structure of the compound, the bodipy core of the compound is planar and the boron atom binds to the two pyrrole nitrogen atoms (N2 and N3) and two fluoride ions with tetrahedral geometry around the boron atom. The B-F and B-N distances are compatible with those of the reported similar compounds [41,64]. In the structure, the meso–4-nitrophenyl group is

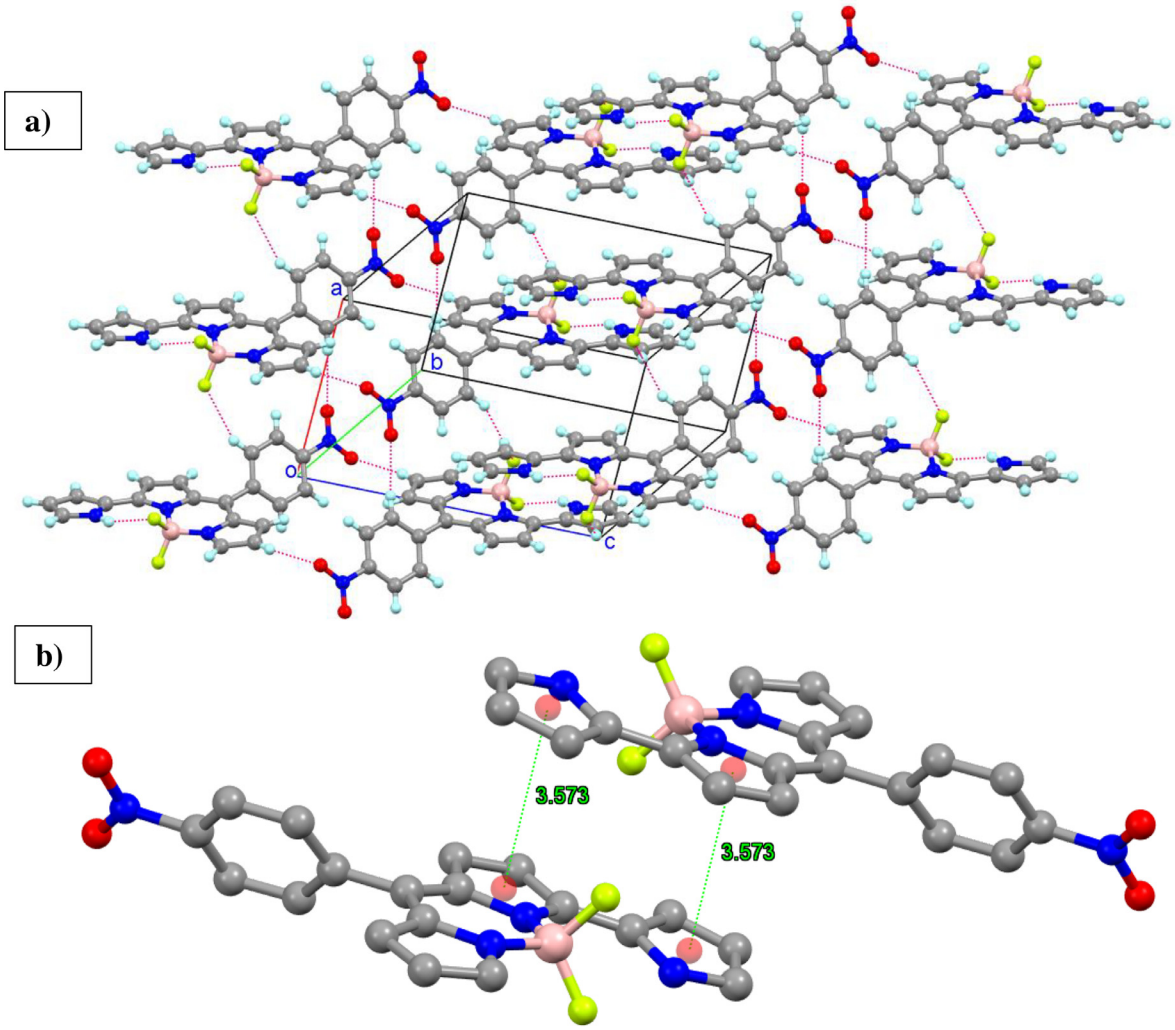

Fig. 3. (a) Packing diagram of compound **3** showing O·····H and F·····H interactions and (b) π-π stacking interactions between the dipyrrin units.

inclined at 54.63° with respect to the bodipy core. The appended pyrrole ring (N1/C4) at the 3-position of the bodipy core is almost co-planar with bodipy core with the dihedral angle of 9.54°. The appended pyrrole group is involved in intra-molecular hydrogen bonding with one of the coordinated fluoride ions (N1-H·····F1).

The Hirshfeld surface for the compound was drawn using Crystal Explorer software in order to examine the intermolecular contacts within the crystal structure [65]. The fingerprint plots showing the different intermolecular contacts are provided in the supplementary documents (Fig. S6). There are two spikes due to the O·····H contacts in the fingerprint plot. In the structure, molecules are linked by O·····H and F·····H interactions and these contacts are seen as red spots in the $d_n$surface. Packing diagram showing the O·····H and F·····H is shown in Fig. 3a. Moreover, there are π-π stacking interactions between the dipyrrin units of the two molecules (Fig. 3b).

3.2. Photophysical properties

Photophysical properties of synthesised BODIPY based compounds **2** and **3** were studied in various solvents with different polarities (Hexane, DCM, EtOH and DMSO) and the data are listed in Table 2. Normalized absorption spectra of compounds are shown Fig. 4. In DCM, compound **2** exhibits a strong absorption maximum at 509 nm and this absorption maximum can be assigned to the S_0-S_1 ($\pi - \pi*$) electronic transition. In comparison with compound **2**, this main absorption maximum red shifted to 586 nm in compound **3**. In the absorption spectrum of 2, 0–1 vibrational transition was observed as a shoulder at around 482 nm. In absorption spectra of compound **3**, the absorption band maximum of this vibronic transition was centered at 550 nm as a separate band. In the absorption spectra of compounds, a broad band observed in the high energy region was attributed to S_0-S_2 ($\pi - \pi*$) electronic transition. This band maximum was located at 331 and 406 nm, respectively, for compounds **2** and **3**.

Normalized emission spectra of the compounds in different solvents are shown Fig. 5. In DCM, compound **2** showed a strong

Table 2
Optical properties of the compound **2** and **3** in various solvents.

Compound	Solvent	λ_{abs}	λ_{em}	Stokes shift	Φ_F
		nm	nm	nm	
2	Hexane	507	528	21	–
	DCM	509	554	45	0.010 [49]
	EtOH	506	526	20	–
	DMSO	510	560	50	–
3					
	Hexane	549, 585	630	45	0.049
	DCM	550, 586	643	57	0.016
	EtOH	547, 583	641	58	–
	DMSO	556, 593	655	62	–

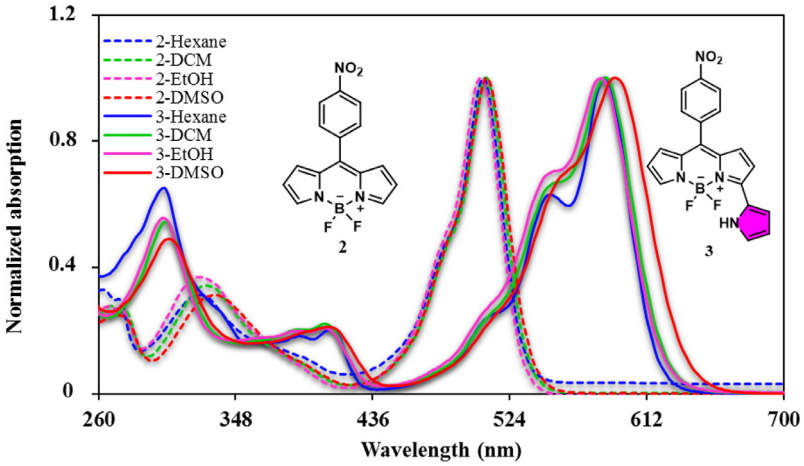

Fig. 4. Normalized absorption spectra of compounds **2** and **3** in various solvents.

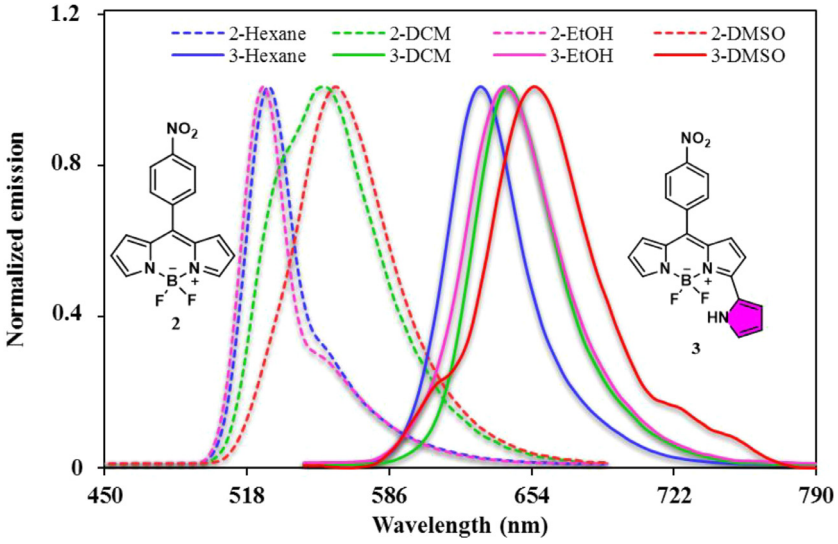

Fig. 5. Absorption spectra of compounds **2** and **3** in various solvents.

emission band between 490 and 690 nm range ($\lambda_{max=}$ 554 nm). The emission band of compound **3** showed a considerable red shift to 550–780 nm range (λ_{max} = 643 nm) in comparison to compound **2**. In DCM, a large bathochromic shift was observed in the absorption and emission band maximum of compound **3** (77 and 89 nm red shifts for absorption and emission, respectively), this can be due to the extension of π-electron delocalization [29] *via* substitution of one pyrrole ring at 3-position of the compound **2**. The substitution of -NO_2 at the meso–aryl group of compound **3** has no effect on this extension of π-electron delocalization because the nitro group is not directly in conjugation with the BODIPY core, it is located at a proximal position [66]. The absorption and emission bands of the compounds were affected by the solvent polarity, when the solvent changed from hexane to DMSO, the absorption and emission maxima red shifted (Table 2). This red shift is consistent with the general behavior of BODIPY dyes [67–69] and represent the polarizability of the solvent [49].

The emission band intensities of compounds decreased dramatically as the solvent polarity increased (Fig. S7), indicating that they exhibit stronger fluorescence in non-polar solvents. The fluorescence quantum yields of compound **3** which were calculated 0.049 and 0.016 in hexane and DCM confirm to this inference. There is a slight increase in the quantum yield of compound **3** compared to compound **2** (Φ_F = 0.010 in DCM). This slight increase may be assigned to the enhanced rigidity of compound **3** due to the intramolecular hydrogen bonding between the appended pyrrole group nitrogen and one of the coordinated fluoride ions (N1-H·····F1) [42]. Compound **3** showed low fluorescence in compared to the other *meso*–substitute derivatives [42,43] because of the free rotation of the *meso*–substituent increasing loss of energy from the excited states via non-irradiated molecular motions and electron-withdrawing effect of the nitro group [5,66,70,71]. Due to the to the strong electron-withdrawing effect of nitro group, the fluorescence of compound **3** can quench via an intramolecular photoinduced electron transfer (PET) process from the excited BODIPY core to the electron-deficient benzene moiety [66].

3.3. Computational results

3.3.1. Optimized structures and frontier molecular orbitals (FMOs)

The optimized structures that determine the space orientation of the atoms in the molecule and the frontier molecules orbitals, which are from their importance in optic and electronic behavior, were calculated in the gas phase at the B3LYP/6–31+*G*(d,p) level. The optimized structures of 2 and 3 molecules and contour diagrams of frontier orbitals, HOMO and LUMO, are given in Fig. 6.

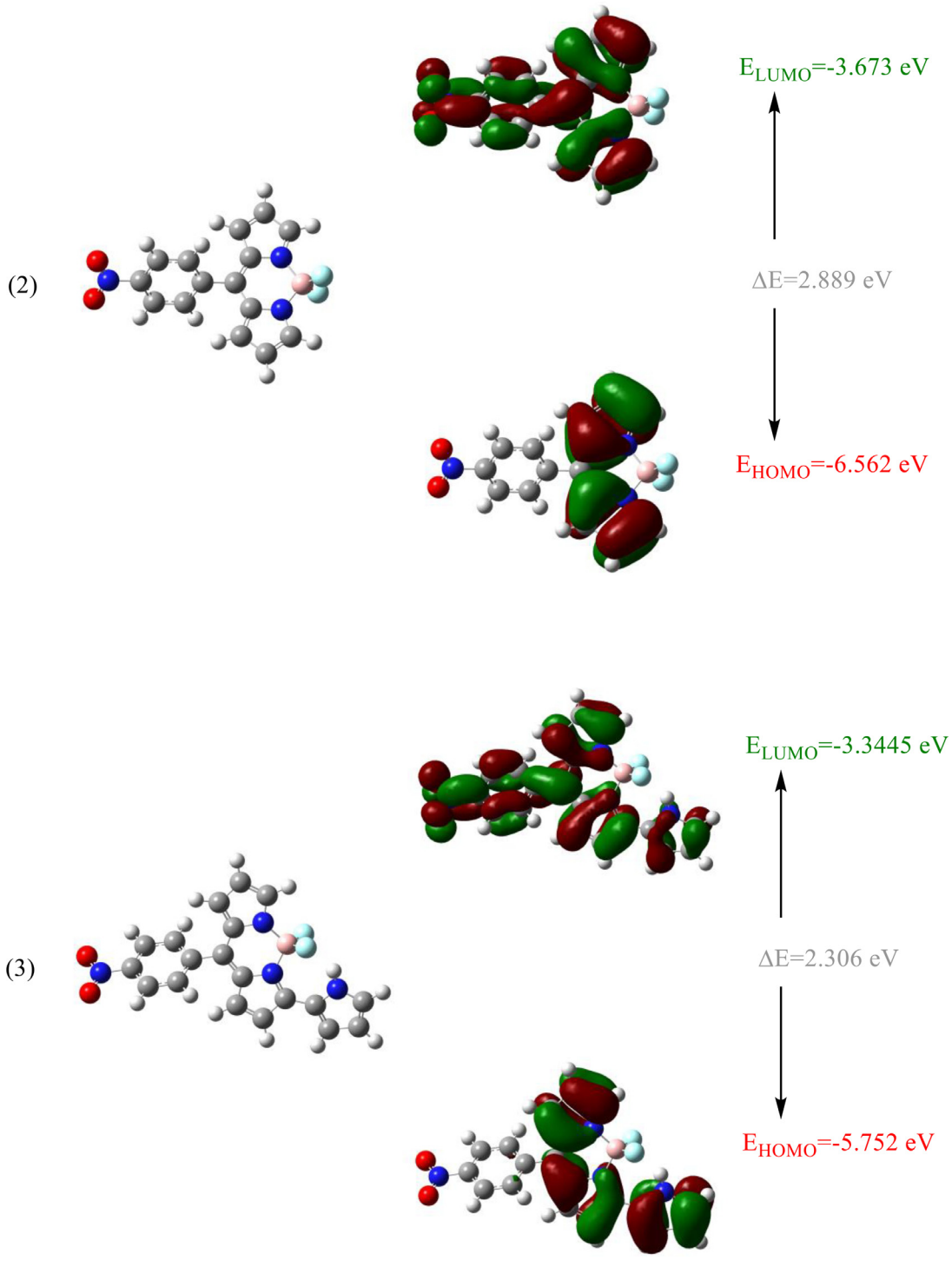

Fig. 6. Optimized structures and contour diagrams of compounds **2** and **3**.

Frontier molecular orbitals (FMOs) are the highest occupied molecular orbital (HOMO) and the lowest unoccupied molecular orbital (LUMO). According to the contour diagrams of the HOMO and LUMO orbitals given in Fig. 6, it shows that the HOMO and LUMO orbitals are localized in the π-bonds of the molecules. The HOMO molecular orbital refers to the electron-donating sites in the molecule. Electron donor atoms in molecules appear on dipyrolo moiety and electron acceptor atoms appear on the π bonds in the molecules 2 and 3.

3.3.2. Non-linear optical (NLO) properties

The nonlinear optical (NLO) properties of organic compounds have been an important research topic because of the conjugated systems and their planarity. Thanks to these features, it has contributed to technological developments such as frequency shifting, optical modulation, switching, logic and memory [72]. It is possible to predict the NLO properties theoretically with computational chemistry methods. Quantum chemical parameters and polarizability parameters (total static dipole moment (μ), the average linear

Table 3
The calculated total static dipole moment(μ), the average linear polarizability (α), the anisotropy of the polarizability ($\Delta\alpha$), first hyperpolarizability (β).

Parameters	Urea	2	3
μ[a]	1.8059	2.0267	3.5091
α[b]	3.6720	17.6311	20.1064
$\Delta\alpha$[d]	8.2365	91.1059	144.3314
β[c]	$6.87\text{x}10^{-28}$	$2.51\text{x}10^{-27}$	$3.43\text{x}10^{-27}$
E_{HOMO}	−7.317	−6.562	−5.752
E_{LUMO}	−0.373	−3.673	−3.445
ΔE	6.944	2.889	2.306

[a] In Debye.
[b] In Å^3.
[c] In cm^5/esu.
[d] eV.

polarizability (α), the anisotropy of the polarizability ($\Delta\alpha$), first hyperpolarizability (β)) are used to predict NLO properties [73]. The total static dipole moment (μ), the average linear polarizability (α), the anisotropy of the polarizability ($\Delta\alpha$), first hyperpolarizability (β) for 2 and 3 are calculated at B3LYP/6–31+G (d,p) level in gas phase and listed in Table 3.

The energy of the HOMO can be related to the NLO properties of the chemical species. A high E_{HOMO} value indicates the tendency of electron transfer to the low vacant molecular orbital of a suitable molecule. A lower E_{LUMO} value indicates a higher electron-accepting ability of the molecule. The NLO properties of the studied molecules increase with increasing HOMO and decreasing LUMO energy values. Moreover, with the effect of electron acceptor and donor groups, the energy gap between LUMO and HOMO decreases, and the NLO properties of the molecules increase [74]. According to the HOMO, LUMO and LUMO-HOMO energies given in Table 3, it can be said that the NLO feature of 3 molecules is more advantageous than the NLO feature of 2 molecules.

The NLO parameters given in Table 3 are compared considering the urea reference material. The increasing values of the total static dipole moment(μ), the average linear polarizability (α), the anisotropy of the polarizability ($\Delta\alpha$) and first hyperpolarizability (β) parameters used to compare the NLO properties provide superiority. According to our results listed in Table 3, among our compounds with ring structure, compound **3** has higher total dipole moment values (3.5091 D) than 2 compound (2.0267 D). It is noteworthy that the total dipole moment values of the 3 molecules are approximately 3 times higher than that of urea, which acts as the reference compound. Similarly, compared to compound **2**, compound **3** shows a remarkable increase in the average linear polarizability and the anisotropy of the polarizability indices, respectively (α = 17.6311 and 20.1064 Å^3 and $\Delta\alpha$ = 91.1059 and 144.3314 Å^3). In addition, in the calculated first hyperpolarizability values, it is seen that compound **2** and **3** compounds have the values of 2.51 x 10^{-27} and 3.43 x10^{-27} cm^5/esu, respectively. The first hyperpolarizability parameters are 10 times higher than that of the urea molecule. Frequently, urea is chosen as one of the prototypical molecules in the study of the NLO behavior of a particular molecular system, thereby often considered the threshold for comparative function [75]. The remarkably large nonlinear optical response of compound **3** molecule may result from the energy band gap (LUMO-HOMO). Increasing the conjugate system in compound **3** will somehow make the charge transfer transition more effective.

In the light of this information, the NLO properties of the compounds examined are more effective than urea, which acts as a reference compound, and the NLO property of compound **3** is more advantageous than compound **2**.

Table 4
The reorganization energies, adiabatic/vertical ionization potentials and electron affinities (all in eV) of (2) and (3) at B3LYP/6–31+G(d,p) level in the gas phase.

	$\lambda_{e\ (eV)}$	$\lambda_{h\ (eV)}$	IPa	IPv	EAa	EAv
2	0.134	0.168	1.493	0.098	0.994	1.085
3	0.104	0.150	1.956	1.157	0.892	0.993

3.3.3. Light emitting properties

One of the main features of OLED materials is that they consist of few layers. The suitability of the OLED material for any of these layers can be predicted by the calculation results. OLED material layers consist of an electron transport layer (ETL), an emitting layer (EL), and a hole transport layer (HTL) between a cathode and an anode [76,77]. In addition to these layers, there is the electron injection layer (EIL) adjacent to the cathode and the hole injection layer (HIL) adjacent to the anode [78–81]. In order to increase the efficiency of OLED devices, it is necessary to improve the ETL and HTL features. The reference material for ETL compounds is tris(8-hydroxyquinoline) aluminum complex (Alq3) [82,83] while the reference material for HTL compounds is N,N'-diphenyl-N,N'-. bis(3-methylphenyl)−1,1′-diphenyl-4,4′-diamine (TPD) [84,85]. A good OLED material should have parameters superior to reference materials.

Instead of the transfer integrals of the Marcus equation, direct reorganization energies are calculated using computational methods and these energies are compared with those of the reference materials. The reorganization energies (λ_e and λ_h) of compounds **2** and **3** were calculated and given in Table 4. It is well known that lower reorganization energy means a higher charge transfer rate. The calculated electron and hole reorganization energies of compound **2** are 0.134 and 0.168 eV, respectively. The calculated electron and hole reorganization energies of compound **3** are 0.104 and 0.150 eV, respectively. The λ_e of compounds **2** and **3** are lower than the reference Alq3 (λe = 0.276 eV) [86] for an ETL material. Therefore, it can be said that compounds **2** and **3** are more advantageous as ETL materials instead of Alq3. It is smaller than the λ_h of TPD (λ_h = 0.290 eV) [87], which is the reference material for the HTL material of compounds **2** and **3**. Compounds **2** and **3** are better than TPD as an HTL compound.

Charge transfer barriers are also important parameters in OLED materials. Charge transfer barriers can be predicted by ionization potentials (IPs) and electron affinities (EAs). As a general rule, smaller IP and larger EA indicate better hole (electron) transfer of holes from the hole (electron) transport layer to the emitter layers [88]. Table 2 shows the adiabatic/vertical ionization potentials (IPa/IPv) and adiabatic/vertical electron affinities (EAa/Eav) values for compounds **2** and **3**. The IPa/v and EAa/v values of compound **2** are 1.493/0.098 eV and 0.994/1.085 eV, respectively. The IPa/v and EAa/v values of compound **3** are 1.956/1.157 eV and 0.892/0.993 eV, respectively. When the results are examined, the IP values of compound **3** are higher than compound **2**. Likewise, the EA values of compound **3** are less than compound **2**. While the pyrrole ring in compound **3** increased the IP values, it decreased the EA values. This may be due to the electron-withdrawing property of the pyrrole ring. According to IP and EA values, compound **2** can be considered as HIL and EIL compound, which should be preferred more than compound **3**.

4. Conclusions

In this study, A BODIPY derivative (compound **2**), substituted with 4-nitrophenyl at *meso* positions and its 3-pyrrole substituted derivative (compound **3**) were prepared and characterized by the spectroscopic and analytical methods. Compound **3** was obtained

as single crystal and its structure was determined by single crystal X-ray diffraction study. Photophysical studies showed that the pyrrole attachment to 3-position of the BODIPY core resulted in a considerable red shift in the emission and absorption band maximum. Also, the absorption and emission bands of compounds were affected by the solvent polarity. Density functional theory (DFT) calculations revealed that the HOMO and LUMO orbitals are localized in the π-bonds of the compounds **2** and **3**. The NLO and OLED properties of compounds **2** and **3** were investigated by quantum calculations and according to IP and EA values, compound **2** can be considered as HIL and EIL compound.

Declaration of Competing Interest

None.

CRediT authorship contribution statement

Hilal Kırpık: Investigation, Methodology, Software, Writing – original draft, Conceptualization. **Sultan Erkan:** Investigation, Data curation, Writing – original draft. **Muhammet Kose:** Methodology, Project administration, Funding acquisition, Supervision, Writing – review & editing.

Acknowledgments

We are grateful to Kahramanmaras Sutcu Imam University Research Unit (Project number: 2020/6–22 M and 2020/1–12D) for the financial support. Furthermore, we would like to thank the Higher Education Council Research Board (YÖK 100/2000 PhD. Scholarship Priority Areas Program “Sensor Technologies”) for granting the Scholarship (to Hilal Kırpık).

Supplementary materials

Supplementary material associated with this article can be found, in the online version, at doi:10.1016/j.molstruc.2021.132090.

References

[1] G. Ulrich, R. Ziessel, A. Harriman, Minireviews fluorescent molecular devices the chemistry of fluorescent BODIPY dyes, versatility unsurpassed 47 (2008) 1184–1201 10.1002/anie.200702070.
[2] N. Boens, V. Leen, W. Dehaen, Fluorescent indicators based on BODIPY, Chem. Soc. Rev. 41 (2012) 1130–1172, doi:10.1039/C1CS15132K.
[3] A.C. Benniston, G. Copley, Lighting the way ahead with boron dipyrromethene (BODIPY) dyes, Phys. Chem. Chem. Phys. 11 (2009) 4124, doi:10.1039/b901383k.
[4] H. Lu, J. Mack, Y. Yang, Z. Shen, Structural modification strategies for the rational design of red/NIR region BODIPYs, Chem. Soc. Rev. 43 (2014) 4778–4823, doi:10.1039/C4CS00030G.
[5] N. Boens, B. Verbelen, W. Dehaen, Postfunctionalization of the BODIPY core: synthesis and spectroscopy, Eur. J. Org. Chem. (2015) 6577–6595 2015, doi:10.1002/ejoc.201500682.
[6] N. Boens, B. Verbelen, M.J. Ortiz, L. Jiao, W. Dehaen, Synthesis of BODIPY dyes through postfunctionalization of the boron dipyrromethene core, Coord. Chem. Rev. (2019) 399, doi:10.1016/j.ccr.2019.213024.
[7] M. Liu, S. Ma, M. She, J. Chen, Z. Wang, P. Liu, S. Zhang, J. Li, Structural modification of BODIPY: improve its applicability, Chin. Chem. Lett. 30 (2019) 1815–1824, doi:10.1016/j.cclet.2019.08.028.
[8] L.Y. Niu, Y.S. Guan, Y.Z. Chen, L.Z. Wu, C.H. Tung, Q.Z. Yang, BODIPY-based ratiometric fluorescent sensor for highly selective detection of glutathione over cysteine and homocysteine, J. Am. Chem. Soc. 134 (2012) 18928–18931, doi:10.1021/ja309079f.
[9] X. Liu, W. Chi, Q. Qiao, S.V. Kokate, E.P. Cabrera, Z. Xu, X. Liu, Y.T. Chang, Molecular mechanism of viscosity sensitivity in BODIPY rotors and application to motion-based fluorescent sensors, ACS Sens. 5 (2020) 731–739, doi:10.1021/acssensors.9b01951.
[10] B. Sui, S. Tang, T. Liu, B. Kim, K.D. Belfield, Novel BODIPY-based fluorescence turn-on sensor for Fe^{3+} and its bioimaging application in living cells, ACS Appl. Mater. Interfaces 6 (2014) 18408–18412, doi:10.1021/am506262u.
[11] C.Y. Chou, S.R. Liu, S.P. Wu, A highly selective turn-on fluorescent sensor for Cu(ii) based on an NSe_2 chelating moiety and its application in living cell imaging, Analyst 138 (2013) 3264, doi:10.1039/c3an00286a.
[12] F.K. Tang, J. Zhu, F.K.W. Kong, M. Ng, Q. Bian, V.W.W. Yam, A.K.W. Tse, Y.C. Tse, K.C.F. Leung, A BODIPY-based fluorescent sensor for the detection of Pt2+ and Pt drugs, Chem. Commun. 56 (2020) 2695–2698, doi:10.1039/D0CC00027B.
[13] İ. Ömeroğlu, S.O. Tümay, S. Makhseed, A. Husain, M. Durmuş, A highly sensitive “ON-OFF-ON” dual optical sensor for the detection of Cu(<scp>ii</scp>) ion and triazole pesticides based on novel BODIPY-substituted cavitand, Daltons Trans. 50 (2021) 6437–6443, doi:10.1039/D1DT00792K.
[14] E. Okutan, S.O. Tümay, S. Yeşilot, Colorimetric fluorescent sensors for hemoglobin based on BODIPY dyes, J. Fluoresc. 26 (2016) 2333–2343, doi:10.1007/s10895-016-1929-6.
[15] Y.S. Marfin, A.V. Solomonov, A.S. Timin, E.V. Rumyantsev, Fluorescent labeling of biomolecules with organic probes, Curr. Med. Chem. 24 (2017) 190–212, doi:10.1021/cr0783840.
[16] Y.S. Marfin, A.V. Solomonov, A.S. Timin, E.V. Rumyantsev, Recent advances of individual BODIPY and BODIPY-based functional materials in medical diagnostics and treatment, Curr. Med. Chem. 24 (2017) 2745–2772, doi:10.2174/0929867324666170601092327.
[17] J. Zhang, N. Wang, X. Ji, Y. Tao, J. Wang, W. Zhao, BODIPY-based fluorescent probes for biothiols, Chem. A Eur. J. 26 (2020) 4172–4192, doi:10.1002/chem.201904470.
[18] T. Kowada, H. Maeda, K. Kikuchi, BODIPY-based probes for the fluorescence imaging of biomolecules in living cells, Chem. Soc. Rev. 44 (2015) 4953–4972, doi:10.1039/C5CS00030K.
[19] S. Kolemen, E.U. Akkaya, Reaction-based BODIPY probes for selective bioimaging, Coord. Chem. Rev. 354 (2018) 121–134, doi:10.1016/j.ccr.2017.06.021.
[20] Y. Ni, J. Wu, Far-red and near infrared BODIPY dyes: synthesis and applications for fluorescent pH probes and bio-imaging, Org. Biomol. Chem. 12 (2014) 3774, doi:10.1039/c3ob42554a.
[21] T.G. Pavlopoulos, M. Shah, J.H. Boyer, Laser action from a tetramethylpyrromethene-BF_2 complex, Appl. Opt. 27 (1988) 4998, doi:10.1364/AO.27.004998.
[22] M.J. Ortiz, I. Garcia-Moreno, A.R. Agarrabeitia, G. Duran-Sampedro, A. Costela, R. Sastre, F. López Arbeloa, J. Bañuelos Prieto, I. López Arbeloa, Red-edge-wavelength finely-tunable laser action from new BODIPY dyes, Phys. Chem. Chem. Phys. 12 (2010) 7804, doi:10.1039/b925561c.
[23] F. López Arbeloa, J. Bañuelos, V. Martínez, T. Arbeloa, I. López Arbeloa, Structural, photophysical and lasing properties of pyrromethene dyes, Int. Rev. Phys. Chem. 24 (2005) 339–374, doi:10.1080/01442350500270551.
[24] S.P. Singh, T. Gayathri, Evolution of BODIPY dyes as potential sensitizers for dye-sensitized solar cells, Eur. J. Org. Chem. (2014) 4689–4707 2014, doi:10.1002/ejoc.201400093.
[25] A. Turksoy, D. Yildiz, E.U. Akkaya, Photosensitization and controlled photosensitization with BODIPY dyes, Coord. Chem. Rev. 379 (2019) 47–64, doi:10.1016/j.ccr.2017.09.029.
[26] D.A. Merkushev, S.D. Usoltsev, Y.S. Marfin, A.P. Pushkarev, D. Volyniuk, J.V. Grazulevicius, E.V. Rumyantsev, BODIPY associates in organic matrices: spectral properties, photostability and evaluation as OLED emitters, Mater. Chem. Phys. 187 (2017) 104–111, doi:10.1016/j.matchemphys.2016.11.053.
[27] M. Poddar, R. Misra, Recent advances of BODIPY based derivatives for optoelectronic applications, Coord. Chem. Rev. 421 (2020) 213462, doi:10.1016/j.ccr.2020.213462.
[28] B.M. Squeo, M. Pasini, BODIPY platform: a tunable tool for green to NIR OLEDs, Supramol. Chem. 32 (2020) 56–70, doi:10.1080/10610278.2019.1691727.
[29] A. Loudet, K. Burgess, BODIPY dyes and their derivatives: syntheses and spectroscopic properties, Chem. Rev. 107 (2007) 4891–4932, doi:10.1021/cr078381n.
[30] M.M. Ravikanth, L. Vellanki, R. Sharma, Functionalized boron-dipyrromethenes and their applications, Rep. Org. Chem. 1 (2016), doi:10.2147/ROC.S60504.
[31] S. Çetindere, Novel water-soluble cyclotriphosphazene-bodipy conjugates : synthesis, Charact. Photophys. Prop. (2019) 1143–1152.
[32] S. Çetindere, S.O. Tümay, A. Kılıç, M. Durmuş, S. Yeşilot, Synthesis and physicochemical properties of cyclotriphosphazene-BODIPY conjugates, Dye Pigment. 139 (2017) 517–523, doi:10.1016/j.dyepig.2016.12.035.
[33] R. Sharma, V. Lakshmi, T. Chatterjee, M. Ravikanth, Effects of five membered aromatic heterocycles at the meso-position on the electronic properties of 3-pyrrolyl BODIPY, New J. Chem. 40 (2016) 5855–5860, doi:10.1039/C6NJ00118A.
[34] T. Kaur, V. Lakshmi, M. Ravikanth, Functionalized 3-pyrrolyl boron-dipyrromethenes, RSC Adv. 3 (2013) 2736, doi:10.1039/c2ra22618a.
[35] M. Ono, H. Watanabe, H. Kimura, H. Saji, BODIPY-based molecular probe for imaging of cerebral β-amyloid plaques, ACS Chem. Neurosci. 3 (2012) 319–324, doi:10.1021/cn3000058.
[36] M. Ono, M. Ishikawa, H. Kimura, S. Hayashi, K. Matsumura, H. Watanabe, Y. Shimizu, Y. Cheng, M. Cui, H. Kawashima, H. Saji, Development of dual functional SPECT/fluorescent probes for imaging cerebral β-amyloid plaques, Bioorg. Med. Chem. Lett. 20 (2010) 3885–3888, doi:10.1016/j.bmcl.2010.05.027.
[37] H. Watanabe, M. Ono, K. Matsumura, M. Yoshimura, H. Kimura, H. Saji, Molecular imaging of β-amyloid plaques with near-infrared boron dipyrromethane (BODIPY)-based fluorescent probes, Mol. Imaging 12 (2013) 7290.2013.00049, doi:10.2310/7290.2013.00049.
[38] W.J. Shi, P.C. Lo, A. Singh, I. Ledoux-Rak, D.K.P. Ng, Synthesis and second-order nonlinear optical properties of push-pull BODIPY derivatives, Tetrahedron 68 (2012) 8712–8718, doi:10.1016/j.tet.2012.08.033.
[39] B. Kulyk, S. Taboukhat, H. Akdas-Kilig, J.L. Fillaut, M. Karpierz, B. Sahraoui, Tuning the nonlinear optical properties of BODIPYs by functionalization with dimethylaminostyryl substituents, Dye Pigment 137 (2017) 507–511, doi:10.1016/j.dyepig.2016.10.045.

[40] B. Kulyk, S. Taboukhat, H. Akdas-Kilig, J.L. Fillaut, Y. Boughaleb, B. Sahraoui, Nonlinear refraction and absorption activity of dimethylaminostyryl substituted BODIPY dyes, RSC Adv. 6 (2016) 84854–84859, doi:10.1039/C6RA19023E.
[41] M.R. Rao, M.D. Tiwari, J.R. Bellare, M. Ravikanth, Synthesis of BF2 complexes of prodigiosin type oligopyrroles, J. Org. Chem. 76 (2011) 7263–7268, doi:10.1021/jo201183s.
[42] M. Zhang, E. Hao, J. Zhou, C. Yu, G. Bai, F. Wang, L. Jiao, Synthesis of pyrrolyldipyrrinato BF2 complexes by oxidative nucleophilic substitution of boron dipyrromethene with pyrrole, Org. Biomol. Chem. 10 (2012) 2139, doi:10.1039/c2ob06689k.
[43] K.J. Kadassery, A. Nimesh, S. Raj, N. Agarwal, 3-/3,5-Pyrrole-substituted BODIPY derivatives and their photophysical and electrochemical studies, J. Chem. Sci. 128 (2016) 1435–1443, doi:10.1007/s12039-016-1134-9.
[44] Thermo Fisher Scientific. Protein Labeling Reagentshttps://www.thermofisher.com/search/browse/category/tr/en/90222235/protein+labeling+reagents. BODIPY™ 576/589, BODIPY™ 650/665-X NHS Ester (Succinimidyl Ester). Accessed October 11, 2021.
[45] A.T.R. Williams, S.A. Winfield, J.N. Miller, Relative fluorescence quantum yields using a computer-controlled luminescence spectrometer, Analyst 108 (1983) 1067, doi:10.1039/an9830801067.
[46] R.F. Kubin, A.N. Fletcher, Fluorescence quantum yields of some rhodamine dyes, J. Lumin. 27 (1982) 455–462, doi:10.1016/0022-2313(82)90045-X.
[47] B.J. Littler, M.A. Miller, C.H. Hung, R.W. Wagner, D.F. O'Shea, P.D. Boyle, J.S. Lindsey, Refined synthesis of 5-substituted dipyrromethanes, J. Org. Chem. 64 (1999) 1391–1396 10.1021/jo982015+.
[48] F. Frank, L.M. Alice, P. Mauker, A.A. Alsimaree, P.G. Waddell, M.R. Probert, T.J. Penfold, J.G. Knight, M.J. Hall, Synthesis of 3,5-dichloro-4,4-difluoro-4-bora-3a,4a-diaza-s-indacenes (BODIPYs) via Cu(OTf)2 mediated oxidative nucleophilic substitution of hydrogen by chloride, Tetrahedron 76 (2020) 131113, doi:10.1016/j.tet.2020.131113.
[49] A.C. Benniston, S. Clift, A. Harriman, Intramolecular charge-transfer interactions in a julolidine-Bodipy molecular assembly as revealed via 13C NMR chemical shifts, J. Mol. Struct. 985 (2011) 346–354, doi:10.1016/j.molstruc.2010.11.018.
[50] O.V. Dolomanov, L.J. Bourhis, R.J. Gildea, J.A.K. Howard, H. Puschmann, OLEX2 : a complete structure solution, refinement and analysis program, J. Appl. Crystallogr. 42 (2009) 339–341, doi:10.1107/S0021889808042726.
[51] G.M. Sheldrick, SHELXT - Integrated space-group and crystal-structure determination, Acta Crystallogr. Sect. A Found. Adv. 71 (2015) 3–8, doi:10.1107/S2053273314026370.
[52] G.M. Sheldrick, Crystal structure refinement with SHELXL, Acta Crystallogr. Sect. C Struct. Chem. 71 (2015) 3–8, doi:10.1107/S2053229614024218.
[53] R.D. Dennington II, T.A. Keith, J.M. Millam, GaussView 5.0, Wallingford CT. (2009).
[54] J. Frisch, G.W. Trucks, H.B. Schlegel, G.E. Scuseria, M.A. Robb, J.R. Cheeseman, G. Scalmani, V. Barone, B. Mennucci, G.A. Petersson, H. Nakatsuji, M. Caricato, X. Li, H.P. Hratchian, A.F. Izmaylov, J. Bloino, G. Zheng, J.L. Sonnenberg, M. Hada, M. Ehara, K. Toyota, R. Fukuda, J. Hasegawa, M. Ishida, T. Nakajima, Y. Honda, O. Kitao, H. Nakai, T. Vreven, J.A. Montgomery, J.E. Peralta, F. Ogliaro, M. Bearpark, J.J. Heyd, E. Brothers, K.N. Kudin, V.N. Staroverov, T. Keith, R. Kobayashi, J. Normand, K. Raghavachari, A. Rendell, J.C. Burant, S.S. Iyengar, J. Tomasi, M. Cossi, N. Rega, J.M. Millam, M. Klene, J.E. Knox, J.B. Cross, V. Bakken, C. Adamo, J. Jaramillo, R. Gomperts, R.E. Stratmann, O. Yazyev, A.J. Austin, R. Cammi, C. Pomelli, J.W. Ochterski, R.L. Martin, K. Morokuma, V.G. Zakrzewski, G.A. Voth, P. Salvador, J.J. Dannenberg, S. Dapprich, A.D. Daniels, O. Farkas, J.B. Foresman, J.V. Ortiz, J. Cioslowski, D.J. Fox, Gaussian, Inc., Wallingford CT. (2010).
[55] S. Erkan, Activity of the rocuronium molecule and its derivatives: a theoretical calculation, J. Mol. Struct. 1189 (2019) 257–264, doi:10.1016/j.molstruc.2019.04.042.
[56] S.A. Gungor, I. Sahin, O. Gungor, S.E. Kariper, F. Tumer, M. Kose, Pamoic acid esters and their xanthene derivatives: flourimetric detection of nitroaromatic compounds and non-linear optical properties, Sens. Actuators B Chem. 255 (2018) 3344–3354, doi:10.1016/j.snb.2017.09.161.
[57] U. Daswani, U. Singh, P. Sharma, A. Kumar, From molecules to devices: a DFT/TD-DFT study of dipole moment and internal reorganization energies in optoelectronically active Aryl Azo chromophores, J. Phys. Chem. C 122 (2018) 14390–14401, doi:10.1021/acs.jpcc.8b04070.
[58] A. Irfan, Modeling of efficient charge transfer materials of 4,6-di(thiophen-2-yl)pyrimidine derivatives: quantum chemical investigations, Comput. Mater. Sci. 81 (2014) 488–492, doi:10.1016/j.commatsci.2013.09.003.
[59] S. Erkan, Theoretical and experimental spectroscopic properties and molecular docking of F8BT p-type semiconducting polymer, Russ. J. Phys. Chem. A 94 (2020) 445–452, doi:10.1134/S0036024420020314.
[60] N. Özkan, S. Erkan, K. Sayın, D. Karakaş, Research on structural, spectral (IR, UV-Vis, 1H- and 13C-NMR) and light emitting properties of triisocyano-based trinuclear Au(I) complexes, Chem. Pap. 74 (2020) 2415–2425, doi:10.1007/s11696-020-01088-3.
[61] A. Irfan, S. Muhammad, A.R. Chaudhry, A.G. Al-Sehemi, R. Jin, Tuning of optoelectronic and charge transport properties in star shaped anthracenothiophene-pyrimidine derivatives as multifunctional materials, Optik 149 (2017) 321–331 (Stuttg), doi:10.1016/j.ijleo.2017.09.065.
[62] H.H. Khalid, S. Erkan, N. Bulut, Halogens effect on spectroscopy, anticancer and molecular docking studies for platinum complexes, Optik 244 (2021) 166324 (Stuttg), doi:10.1016/j.ijleo.2021.166324.
[63] E.V. de Wael, J.A. Pardoen, J.A. van Koeveringe, J. Lugtenburg, Pyrromethene-BF 2 complexes (4,4′-difluoro-4-bora-3a,4a-diaza- s -indacenes). Synthesis and luminescence properties, Recl. Des. Trav. Chim. Des. Pays Bas. 96 (1977) 306–309, doi:10.1002/recl.19770961205.
[64] E. Dai, W. Pang, X.F. Zhang, X. Yang, T. Jiang, P. Zhang, C. Yu, E. Hao, Y. Wei, X. Mu, L. Jiao, Synthesis and photophysics of BF 2 -rigidified partially closed chain bromotetrapyrroles: near infrared emitters and photosensitizers, Chem. An Asian J. 10 (2015) 1327–1334, doi:10.1002/asia.201500118.
[65] M.A. Spackman, D. Jayatilaka, Hirshfeld surface analysis, CrystEngComm 11 (2009) 19–32, doi:10.1039/B818330A.
[66] T. Ueno, Y. Urano, H. Kojima, T. Nagano, Mechanism-based molecular design of highly selective fluorescence probes for nitrative stress, J. Am. Chem. Soc. 128 (2006) 10640–10641, doi:10.1021/ja061972v.
[67] W. Qin, M. Baruah, M. Van der Auweraer, F.C. De Schryver, N. Boens, Photophysical properties of borondipyrromethene analogues in solution, J. Phys. Chem. A 109 (2005) 7371–7384, doi:10.1021/jp052626n.
[68] H.L. Kee, C. Kirmaier, L. Yu, P. Thamyongkit, W.J. Youngblood, M.E. Calder, L. Ramos, B.C. Noll, D.F. Bocian, W.R. Scheidt, R.R. Birge, J.S. Lindsey, D. Holten, Structural control of the photodynamics of boron−dipyrrin complexes, J. Phys. Chem. B 109 (2005) 20433–20443, doi:10.1021/jp0525078.
[69] M. Kollmannsberger, K. Rurack, U. Resch-Genger, J. Daub, Ultrafast charge transfer in amino-substituted boron dipyrromethene dyes and its inhibition by cation complexation: a new design concept for highly sensitive fluorescent probes, J. Phys. Chem. A 102 (1998) 10211–10220, doi:10.1021/jp982701c.
[70] G.J. Hedley, A. Ruseckas, A. Harriman, I.D.W. Samuel, Conformational effects on the dynamics of internal conversion in boron dipyrromethene dyes in solution, Angew. Chem. 123 (2011) 6764–6767, doi:10.1002/ange.201101219.
[71] S. Toliautas, J. Dodonova, A. Žvirblis, I. Čiplys, A. Polita, A. Devižis, S. Tumkevičius, J. Šulskus, A. Vyšniauskas, Enhancing the viscosity-sensitive range of a BODIPY molecular rotor by two orders of magnitude, Chem. A Eur. J. 25 (2019) 10342–10349, doi:10.1002/chem.201901315.
[72] M. Kose, G. Ceyhan, D. Karakaş, Synthesis, characterization and nonlinear optical properties of two mononuclear Cu(II) complexes of 2,6-bis(1-butylbenzimidazol-2-yl)pyridine, J. Coord. Chem. 69 (2016) 497–507, doi:10.1080/00958972.2015.1134789.
[73] S. Erkan, D. Karakaş, A theoretical study on cyclometalated iridium (III) complexes by using a density functional theory, J. Theor. Comput. Chem. 19 (2020) 2050006, doi:10.1142/S0219633620500066.
[74] S. Erkan, D. Karakaş, Computational investigation of structural, nonlinear optical and anti-tumor properties of dinuclear metal carbonyls bridged by pyridyl ligands with alkyne unit, J. Mol. Struct. 1199 (2020) 127054, doi:10.1016/j.molstruc.2019.127054.
[75] M. Sarigul, S.E. Kariper, P. Deveci, H. Atabey, D. Karakas, M. Kurtoglu, Multi-properties of a new azo-Schiff base and its binuclear copper(II) chelate: preparation, spectral characterization, electrochemical, potentiometric and modeling studies, J. Mol. Struct. 1149 (2017) 520–529, doi:10.1016/j.molstruc.2017.08.016.
[76] Y. Li, Q. Wei, L. Cao, F. Fries, M. Cucchi, Z. Wu, R. Scholz, S. Lenk, B. Voit, Z. Ge, S. Reineke, Organic light-emitting diodes based on conjugation-induced thermally activated delayed fluorescence polymers: interplay between intra- and intermolecular charge transfer states, Front. Chem. 7 (2019), doi:10.3389/fchem.2019.00688.
[77] P. Chulkin, O. Vybornyi, M. Lapkowski, P.J. Skabara, P. Data, Impedance spectroscopy of OLEDs as a tool for estimating mobility and the concentration of charge carriers in transport layers, J. Mater. Chem. C 6 (2018) 1008–1014, doi:10.1039/C7TC04599A.
[78] B. Zhao, H. Wang, C. Han, P. Ma, Z. Li, P. Chang, H. Xu, Highly efficient deep-red non-doped diodes based on a T-shape thermally activated delayed fluorescence emitter, Angew. Chem. Int. Ed. 59 (2020) 19042–19047, doi:10.1002/anie.202008885.
[79] Y. Chen, J. Zhu, Y. Wu, J. Yao, D. Yang, X. Qiao, Y. Dai, Q. Tong, D. Ma, Highly efficient fluorescence/phosphorescence hybrid white organic light-emitting devices based on a bipolar blue emitter to precisely control charges and excitons, J. Mater. Chem. C 8 (2020) 7543–7551, doi:10.1039/D0TC01549K.
[80] H. Zhou, S. Guo, X. Jin, J. Cao, J. Cui, Z. Zhao, J. Huang, J. Su, Novel hole transport materials based on triphenylvinyl substituted triarylamine with excellent thermal stability for green OLEDs, Dye Pigment 195 (2021) 109641, doi:10.1016/j.dyepig.2021.109641.
[81] Y.C. Chen, J.H. Yen, Y.J. Wang, C.A. Hsieh, L.Y. Chen, Light extraction enhancement in organic light-emitting diodes through polyimide/porous silica hybrid films, Org. Electron. 95 (2021) 106213, doi:10.1016/j.orgel.2021.106213.
[82] S. Niu, J. Cai, G. Wang, Two-dimensional MOS_2 for hydrogen evolution reaction catalysis: the electronic structure regulation, Nano Res. 14 (2021) 1985–2002, doi:10.1007/s12274-020-3249-z.
[83] A. Üngördü, Charge transfer properties of Gaq3 and its derivatives: an OLED study, Chem. Phys. Lett. 733 (2019) 136696, doi:10.1016/j.cplett.2019.136696.
[84] R. Reyes, E. Hering, M. Cremona, C.F. da Silva, H. Brito, C. Achete, Growth and characterization of OLED with samarium complex as emitting and electron transporting layer, Thin Solid Films (2002) 23–29 420-421, doi:10.1016/S0040-6090(02)00651-X.
[85] H. Murata, H. Mattoussi, C.D. Merritt, Y. Iizumi, J. Kido, H. Tokuhisa, T. Tsutsui, Z.H. Kafafi, Molecular organic light-emitting diodes based on a guest-host active layer: approaches for enhancing device performance, Mol. Cryst. Liq. Cryst. Sci. Technol. Sect. A. Mol. Cryst. Liq. Cryst. 353 (2000) 567–580, doi:10.1080/10587250008025690.

[86] A. Lukyanov, C. Lennartz, D. Andrienko, Amorphous films of tris(8-hydroxyquinolinato)aluminium: force-field, morphology, and charge transport, Phys. Status Solidi. 206 (2009) 2737–2742, doi:10.1002/pssa.200925276.
[87] N.E. Gruhn, D.A. da Silva Filho, T.G. Bill, M. Malagoli, V. Coropceanu, A. Kahn, J.L. Brédas, The vibrational reorganization energy in pentacene: molecular influences on charge transport, J. Am. Chem. Soc. 124 (2002) 7918–7919, doi:10.1021/ja0175892.
[88] J. Gao, J. Li, X. Li, D. Han, P. Guo, X. Zhu, X. Shang, Theoretical investigation on the effect of the modification of 2-phenylpyridine ligand on the photophysical properties for a series of iridium(III) complexes with carbazate ancillary ligands, J. Lumin. 209 (2019) 365–371, doi:10.1016/j.jlumin.2019.01.054.